*Inorg. Chem.* **2008**, *47*, 10232−10245

# One-Dimensional Iron(II) Compounds Exhibiting Spin Crossover and Liquid Crystalline Properties in the Room Temperature Region

**M. Seredyuk,[†] A. B. Gaspar,*[,‡] V. Ksenofontov,[†] Y. Galyametdinov,[§] M. Verdaguer,[||] F. Villain,[||] and P. Gütlich*[,†]**

*Institut für Anorganische and Analytische Chemie, Johannes-Gutenberg-Universität, Staudinger-Weg 9, D-55099 Mainz, Germany, Institut de Ciència Molecular/Departament de Química Inorgànica, Universitat de València, Edifici d'Instituts de Paterna, Apartat de Correus 22085, 46071 València, Spain, Kazan Physical Technical Institute, Russian Academy of Science, Sibirsky Tract 10/7, 420029, Kazan (Russia), and Laboratoire de Chimie Inorganique et Matériaux Moléculaires, UMR-CNRS 7071, FR-CNRS 2769, Université Pierre et Marie Curie, 4 place Jussieu, case courrier 42, 75252 Paris Cedex 05, France*

Received April 7, 2008

A novel series of 1D Fe(II) metallomesogens have been synthesized using the ligand 5-bis(alkoxy)-*N*-(4*H*-1,2,4-triazol-4-yl)benzamide ($C_n$-tba) and the $Fe(X)_2 \cdot sH_2O$ salts. The polymers obey the general formula $[Fe(C_n\text{-tba})_3](X)_2 \cdot sH_2O$ [$X = CF_3SO_3^-$, $BF_4^-$; $n = 4, 6, 8, 10, 12$]. The derivatives with $n = 4, 6$ exhibit spin transition behavior like in crystalline compounds, whereas those with $n = 8, 10, 12$ present a spin transition coexisting with the mesomorphic behavior in the room-temperature region. A columnar mesophase has been found for the majority of the metallomesogens, but also a columnar lamellar mesophase was observed for other derivatives. $[Fe(C_{12}\text{-tba})_3](CF_3SO_3)_2$ represents a new example of a system where the phase transition directly influences the spin transition of the Fe(II) ions but is not the driving energy of the spin crossover phenomenon. The compounds display drastic changes of color from violet (low-spin state, LS) to white (high-spin state, HS). The compounds are fluid, and it is possible to prepare thin films from them.

## Introduction

Spin crossover metallomesogens are a new type of bifunctional materials exhibiting spin crossover (SCO)[1] and liquid crystalline (LC) properties.[2] SCO materials change reversibly their magnetic, structural, dielectric, and optical properties in response to external stimuli such as variation of temperature, pressure, or light irradiation.[1] This change of properties occurs in a very narrow interval of temperatures and/or pressures for cooperative phase transitions. The vast majority of SCO compounds reported so far concerns Fe(II) and Fe(III) complexes, to a lesser extent Co(II), and only in a few cases Mn(III) and Cr(II) complexes.[1a] The interest in tailoring metallomesogens[3] that incorporate electronic bistability lies in the necessity for color in a number of applications in liquid crystals such as passive blocking filters, laser addressed devices, and polarizers based on dichroic effects or in the utility of thermochromism and photochromism.[3–8] Besides, there is a growing interest in processing spin crossover materials in the form of thin films (by exploiting the ability of liquid crystals to form thin layers); the present systems seem to be good candidates for enhancement of spin transition signals, for switching and for sensing in different temperature intervals.[1b,c]

The number of SCO metallomesogens is scarce. A few examples of Fe(III),[9] Co(II),[10] and Fe(II)[11–14] have been reported so far. However, a very rich interplay and synergy between spin transition and liquid-crystal phase transition have been observed: (i) the systems with coupled SCO and phase transitions are subdivided in two groups *a* and *b* (in *a*

* To whom correspondence should be addessed. E-mail: ana.b.gaspar@uv.es.
[†] Johannes-Gutenberg-Universität.
[‡] Universitat de València.
[§] Russian Academy of Science.
[||] Université Pierre et Marie Curie.

(1) (a) Gütlich, P.; GoodwinH. A. Spin Crossover in Transition Metal Compounds, *Top. Curr. Chem.* 2004, Vols. *233, 234, 235*. (b) Gaspar, A. B.; Ksenofontov, V.; Seredyuk, M.; Gütlich, P. *Coord. Chem. Rev.* **2005**, *249*, 2661–2676. (c) Real, J. A.; Gaspar, A. B.; Muñoz, M. C. *Dalton Trans.* **2005**, 2062–2079. (d) Real, J. A.; Gaspar, A. B.; Niel, V.; Muñoz, M. C. *Coord. Chem. Rev.* **2003**, *236*, 121–141. (e) Gütlich, P.; Hauser, A.; Spiering, H. *Angew. Chem., Int. Ed. Engl.* **1994**, *33*, 2024–2054.



10.1021/ic8006266 CCC: $40.75 
Published on Web 07/25/2008

the structural changes associated to the crystal ↔ liquid crystal (Cr ↔ LC) phase transition drives the SCO transition, whereas in *b* the structural changes influence the spin state of the metallic centers but they are not the driving energy of the SCO transition);[13,14] (ii) the systems with both SCO and phase transition in the same temperature region, which are uncoupled,[12] and (iii) the systems with SCO and phase transition in different temperature regions, which are uncoupled.[9–11]

During the last years, we have investigated the possibility to synchronize both transitions, spin transition, and crystalline solid−liquid crystal transition, in Fe(II) complexes.[12–14] The first step in the tailoring of these multifunctional materials has been the choice of SCO systems, showing abrupt spin transition near to or above room temperature. This is the range of temperatures at which usually the LC phase transition is observed. The second step in this approach has focused on the incorporation of the LC moiety into the original SCO systems. Among the synthesized Fe(II) metallomesogens those of type (ii) which display thermochromic properties are based on the 3,5-bis(alkoxy)-*N*-(4*H*-1,2,4-triazol-4-yl)benzamide ligand ($C_n$-tba). In compounds $[Fe(C_n\text{-tba})_3](4\text{-}MeC_6H_4SO_3)_2 \cdot sH_2O$ ($n = 8, 10, 12$; $s = 0, 1$),[12a,b] spin-state change occurs upon dehydration in the room-temperature range where the materials show a columnar mesophase. For the anhydrous materials, $[Fe(C_n\text{-trz})_3](4\text{-}MeC_6H_4SO_3)_2$, a thermally driven spin-state transition is observed in the interval of 280−325 K. Structural data evidenced a columnar organization in the temperature interval of 200−475 K. The obtention of the crystalline state of these materials is difficult. In fact, no melting point has been observed. Therefore, it has been concluded that the spin transition behavior in these metallomesogens is not driven by the phase transition from the crystalline state to the liquid-crystal state but rather by the classical factors, which determines the ligand field strength and the SCO behavior, namely, subtle structural and electronic modifications tuned by the crystal packing. However, in the anhydrous materials an influence of the mesophase in the thermally driven spin-state change was not excluded because it seems to be responsible for the appearance of the hysteresis loops in the spin transition curves derived from magnetic susceptibility measurements.

Here, we present a detailed analysis of the spin transition and of the mesomorphic behavior of novel 1D Fe(II) metallomesogens with the ligand $C_n$-tba of general formula $[Fe(C_n\text{-tba})_3](X)_2 \cdot sH_2O$ [$X = CF_3SO_3^-$, $BF_4^-$; $n = 4, 6, 8, 10, 12$; $s = 0, 0.5, 1$ (below)].

## Results

The compounds $[Fe(C_n\text{-tba})_3](X)_2 \cdot sH_2O$ [$X = CF_3SO_3^-$, $n = 4, 6, 8, 10, 12$, ($\mathbf{C}_n$-1); $s = 0.5$; $X = BF_4^-$, $n = 4, 6, 8, 10, 12$; $s = 1$ ($\mathbf{C}_n$-3)] were synthesized using the $C_n$-tba ligands and the $Fe(X)_2 \cdot 6H_2O$ salts following the synthetic procedure described in the Experimental Section. The nomenclature $\mathbf{C}_n$-N was chosen to label the alkylated complexes, where $\mathbf{C}_n$ represents the alkyl substituents with *n* carbon atoms ($C_nH_{2n+1}$), and N corresponds to the type of anion along with the water of crystallization. Compounds $\mathbf{C}_n$-1 and $\mathbf{C}_n$-2 are pristine ($s = 0.5$) and anhydrous derivatives, respectively, with the anion triflate anion ($CF_3SO_3^-$), and $\mathbf{C}_n$-3 ($s = 1$) and $\mathbf{C}_n$-4 (anhydrous) with the tetrafluoroborate anion ($BF_4^-$). In Chart 1 are shown the codes and the composition of the compounds presented here. The anhydrous compounds, $\mathbf{C}_n$-2 and $\mathbf{C}_n$-4, were obtained by dehydration of the pristine compounds $\mathbf{C}_n$-1 and $\mathbf{C}_n$-3 either in the evacuated flask at 400 K during 15 min or in the SQUID susceptometer, keeping the compounds at 400 K under vacuum during 15 min.

XANES and EXAFS data of $\mathbf{C}_{12}$-1. The interpretation of the XANES and EXAFS spectra of $\mathbf{C}_{12}$-1 is very similar to that of the precursor complex $[Fe(tba)_3](CF_3SO_3)_2 \cdot 2H_2O$.[15]


(2) (a) Laschat, S.; Baro, A.; Steinke, N.; Giesselmann, F.; Hägele, C.; Scalia, G.; Judele, R.; Kapatsina, E.; Sauer, S.; Schreivogel, A.; Tosoni, M. *Angew. Chem., Int. Ed.* **2007**, *46*, 4832–4887, and references therein. (b) Donnio, B.; Guillon, D. *Adv. Polym. Sci.* **2006**, *201*, 45–155. (c) Camerel, F.; Donnio, B.; Bourgogne, C.; Schmutz, M.; Guillon, D.; Davidson, P.; Ziessel, R. *Chem.—Eur. J.* **2006**, *16*, 4261–4274. (d) Reddy, R. A.; Tschierske, C. *J. Mater. Chem* **2006**, *10*, 907–961. (e) Binnemans, K. *Chem. Rev.* **2005**, *11*, 4148–4204. (f) Paleos, C. M.; Tsiourvas, D. *Angew. Chem., Int. Ed.* **1995**, *16*, 1696–1711.

(3) (a) Serrano, J. L. *Metallomesogens (VCH)* 1996, andreferences therein. (b) Hudson, S. A.; Maitlis, P. M. *Chem. Rev.* **1993**, *93*, 861. (c) Donnio, B.; Bruce, D. W. *Struct. Bonding (Berlin)* **1999**, *95*, 193–247. (d) Lemieux, R. P. *Acc. Chem. Res.* **2001**, *34*, 845–853. (e) Gimenez, R.; Lydon, D. P.; Serrano, J. L. *Curr. Opin. Solid State Mater. Sci.* **2002**, *6*, 527–535. (f) Serrano, J. L.; Sierra, T. *Coord. Chem. Rev.* **2003**, *242*, 73–85. (g) Donnio, B. *Curr. Opin. Colloid, Interface Science State Mater. Sci.* **2002**, *7*, 371–394. (h) Bruce, D. W. *Acc. Chem. Res.* **2000**, *33*, 831–840. (i) Piguet, C.; Bünzli, J. C. G.; Donnio, B.; Guillon, D. *Chem. Commun.* **2006**, *36*, 3755–3768. (j) Rowan, S. J. *Angew. Chem., Int. Ed.* **2005**, *44*, 4830–4832.

(4) Shvartsman, F. P.; Krongauz, V. A. *Nature (London)* **1984**, *309*, 608–611.

(5) (a) Bruce, D. W.; Dunmur, P. A.; Esteruelas, M. A.; Hunt, S. E.; Maitlis, P. M.; Marsden, J. R.; Sola, E.; Stacey, J. M. *J. Mater. Chem.* **1991**, *1*, 251–255. (b) Ohta, K.; Hasabe, H.; Moriya, M.; Fujimoto, T.; Yamamoto, I. *J. Mater. Chem.* **1991**, *1*, 831–834. (c) Gregg, B. A.; Fox, M. A.; Bard, A. J. *J. Phys. Chem.* **1989**, *93*, 4227–4234.

(6) De Filpo, G.; Nicoletta, F. P.; Chidichimo, G. *Adv. Mater.* **2005**, *17*, 1150–1152.

(7) Aldred, M. P.; Contoret, A. E. A.; Farrar, S. R.; Stephen, M. K.; Mathieson, D.; O'Neill, M.; Tsoi, W. C.; Vlachos, P. *Adv. Mater.* **2005**, *17*, 1368–1372.

(8) (a) Frogoli, M.; Mehl, G. H. *Chem. Phys. Chem.* **2003**, *1*, 101–103. (b) Irie, M. *Chem. Rev.* **2000**, *100*, 1685.

(9) Galyametdinov, Y.; Ksenofontov, V.; Prosvirin, A.; Ovchinnikov, I.; Ivanova, G.; Gütlich, P.; Haase, W. *Angew. Chem., Int. Ed.* **2001**, *40*, 4269–4271.

(10) (a) Hayami, S.; Danjobara, K.; Inoue, K.; Ogawa, Y.; Matsumoto, N.; Maeda, Y. *Adv. Mater.* **2004**, *16*, 869–872. (b) Hayami, S.; Motokawa, N.; Shuto, A.; Masuhara, N.; Someya, T.; Ogawa, Y.; Inoue, K.; Maeda, Y. *Inorg. Chem.* **2007**, *46*, 1789–1794. (c) Hayami, S.; Moriyama, R.; Shuto, A.; Maeda, Y.; Ohta, K.; Inoue, K. *Inorg. Chem.* **2007**, *46*, 7692–7694.

(11) Hayami, S.; Motokawa, N.; Shuto, A.; Moriyama, R.; Masuhara, N.; Inoue, K.; Maeda, Y. *Polyhedron* **2007**, *26*, 2375–2380.

(12) (a) Seredyuk, M.; Gaspar, A. B.; Ksenofontov, V.; Reiman, S.; Galyametdinov, Y.; Haase, W.; Rentschler, E.; Gütlich, P. *Chem. Mater.* **2006**, *18*, 2513–2519. (b) Seredyuk, M.; Gaspar, A. B.; Ksenofontov, V.; Reiman, S.; Galyametdinov, Y.; Haase, W.; Rentschler, E.; Gütlich, P. *Hyperfine Interact.* **2005**, *166*, 385–390. (c) Fujigaya, T.; Jiang, D. L.; Aida, T. *J. Am. Chem. Soc.* **2003**, *125*, 14690.

(13) Seredyuk, M.; Gaspar, A. B.; Ksenofontov, V.; Galyametdinov, Y.; Kusz, J.; Gütlich, P. *J. Am. Chem. Soc.* **2008**, *130*, 1431–1439.

(14) Seredyuk, M. Gaspar, A. B. Ksenofontov, V., Galyametdinov, Y. Kusz, J. Gütlich, P. *Adv. Funct. Mat.* 2008, adfm.200800049, in press.

(15) Seredyuk, M.; Gaspar, A. B.; Muñoz, M. C.; Verdaguer, M.; Villain, F.; Gütlich, P. *Eur. J. Inorg. Chem.* **2007**, 4481–4491.

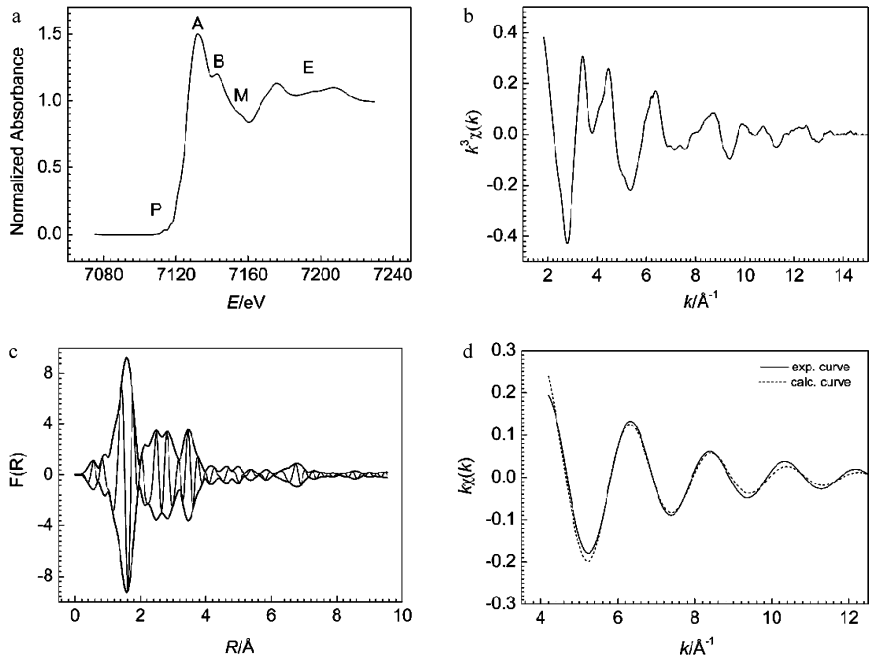


**Figure 1.** Complex $\mathbf{C}_{12}$-1: (a) Edge spectrum at 80 K. P, pre-edge; A, top of the edge; B and M, shoulders; E, EXAFS oscillations; (b) weighted EXAFS signal $k^3\chi(k)$; (c) modulus and imaginary parts of the Fourier transform of the EXAFS signal at 80 K; (d) comparison of the experimental and calculated $k\chi(k)$ values for the first filtered shell.

**Chart 1.** Schematic Polymeric Structure and Composition of $\mathbf{C}_n$-1, $\mathbf{C}_n$-2, $\mathbf{C}_n$-3, and $\mathbf{C}_n$-4 ($n$ = 4, 6, 8, 10, 12)

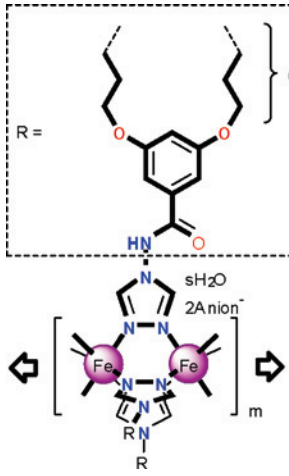


| Anion | s | Compound |
|---|---|---|
| $CF_3SO_3^-$ | 0.5 | $\mathbf{C}_4$-1, $\mathbf{C}_6$-1, $\mathbf{C}_8$-1, $\mathbf{C}_{10}$-1, $\mathbf{C}_{12}$-1 |
| | 0 | $\mathbf{C}_4$-2, $\mathbf{C}_6$-2, $\mathbf{C}_8$-2, $\mathbf{C}_{10}$-2, $\mathbf{C}_{12}$-2 |
| $BF_4^-$ | 1 | $\mathbf{C}_4$-3, $\mathbf{C}_6$-3, $\mathbf{C}_8$-3, $\mathbf{C}_{10}$-3, $\mathbf{C}_{12}$-3 |
| | 0 | $\mathbf{C}_4$-4, $\mathbf{C}_6$-4, $\mathbf{C}_8$-4, $\mathbf{C}_{10}$-4, $\mathbf{C}_{12}$-4 |

The normalized XANES spectrum of $\mathbf{C}_{12}$-1 recorded at 80 K at the iron $K$-edge is typical for an octahedral complex of Fe(II) (part a of Figure 1). It includes absorption in the pre-edge region P assigned to the symmetry-forbidden electronic dipolar transitions from 1s to molecular levels implying 3d orbitals.[16] The first strong absorption (peak A) is located at 7130 eV and can be attributed to a metal 1s to molecular levels implying 4p orbitals dipole-allowed transition.[16] Further, intense shoulders B and M with energies 7142 and 7154 eV, respectively, are due to multiple scattering processes.[17] Finally, absorption in the E region corresponds to the first EXAFS oscillations. The EXAFS oscillation at relatively high energy (7205 eV) evidences short Fe−N distances and the low-spin character of the iron ion. The EXAFS spectrum measured at 80 K is shown in part b of Figure 1, and the Fourier transform of it is displayed in part c of Figure 1. The EXAFS signal provides direct information about the radial distribution of the neighboring atoms around the absorbing atom. The data are very similar to previous EXAFS studies with similar materials (changing the triazole ligand and the counterions) demonstrating the linear local structure.[18–22] The Fourier transform at 80 K consists of five

(16) Real, J. A.; Castro, I.; Bousseksou, A.; Verdaguer, M.; Burriel, R.; Castro, M.; Linares, J.; Varret, F. *Inorg. Chem.* **1997**, *36*, 455–464.
(17) Hannay, C.; Hubin-Franskin, M. J.; Grandjean, F.; Briois, V.; Itie, J. P.; Polian, A.; Trofimenko, S.; Long, G. J. *Inorg. Chem.* **1997**, *36*, 5580–5588.
(18) Yokoyama, T.; Murakami, Y.; Kiguchi, M.; Komatsu, T.; Kojima, N. *Phys. Rev. B: Condens. Matter* **1998**, *58*, 14238–14244.
(19) Erenburg, S. B.; Bausk, N. V.; Varnek, V. A.; Lavrenova, L. G. *J. Magn. Magn. Mater.* **1996**, *158*, 595–596.
(20) Erenburg, S. B.; Bausk, N. V.; Lavrenova, L. G.; Mazalov, L. N. *Nucl. Instrum. Methods Phys. Res., Sect. A* **2000**, *448*, 351–357.
(21) Erenburg, S. B.; Bausk, N. V.; Lavrenova, L. G.; Mazalov, L. N. *J. Magn. Magn. Mater.* **2001**, *226*, 1967–1969.
(22) Michalowicz, A.; Moscovici, J.; Ducourant, B.; Cracco, D.; Kahn, O. *Chem. Mater.* **1995**, *7*, 1833–1842.

**Table 1.** Interlayer Distances $d$ and Thermodynamic Parameters of Spin Transition Derived from the DSC Data for $\mathbf{C}_n$-1 and $\mathbf{C}_n$-3

| compound | $d$/Å, 293 K | thermal transitions/K[a] | $\Delta H^{SCO}$/kJ mol$^{-1}$[c] | $\Delta S^{SCO}$/J K$^{-1}$ mol$^{-1}$ |
|---|---|---|---|---|
| $\mathbf{C}_4$-1 | 24.8 | $Cr\left(LS \underset{283}{\overset{291}{\rightleftharpoons}} HS\right)\overset{510}{\rightarrow}d$ | 14.3 | 49.2 |
| $\mathbf{C}_6$-1 | 23.0 | $Cr\left(LS \underset{309}{\overset{312}{\rightleftharpoons}} HS\right)\overset{510}{\rightarrow}d$ | 14.6 | 46.6 |
| $\mathbf{C}_8$-1 | 24.1 | $Col_L\left(LS \underset{304}{\overset{312}{\rightleftharpoons}} HS\right)\overset{514}{\rightarrow}d$ | 15.3 | 49.4 |
| $\mathbf{C}_{10}$-1 | 29.1 | $g\overset{271}{\rightarrow}Col_h\left(LS \underset{294}{\overset{299}{\rightleftharpoons}} HS\right)\overset{514}{\rightarrow}d$ | 14.9 | 48.2 |
| $\mathbf{C}_{12}$-1 | 29.8 | $g\overset{273}{\rightarrow}Col_h\left(LS \underset{293}{\overset{297}{\rightleftharpoons}} HS\right)\overset{507}{\rightarrow}d$ | 14.2 | 48.1 |
| $\mathbf{C}_4$-3 | 22.6 | $Cr_1\left(LS \underset{255}{\overset{264}{\rightleftharpoons}} HS\right)\underset{370}{\overset{400}{\rightleftharpoons}}Cr_2\overset{450}{\rightarrow}d$ | 17.8 | 68.7 |
| $\mathbf{C}_6$-3 | 24.5 | $Cr_1\left(LS \overset{191}{\rightarrow} HS^b\right)\overset{350}{\rightarrow}Cr_2\overset{456}{\rightarrow}d$ | 11.7[d] | 58.5[d] |
| $\mathbf{C}_8$-3 | 27.6 | $Col_h\left(LS \overset{256}{\rightarrow} HS^b\right)\overset{458}{\rightarrow}d$ | 4.6[d] | 17.8[d] |
| $\mathbf{C}_{10}$-3 | 30.3 | $G\left(LS \underset{263}{\overset{270}{\rightleftharpoons}} HS\right)\overset{300}{\rightarrow}Col_h\overset{479}{\rightarrow}d$ | 5.2 | 19.8 |
| $\mathbf{C}_{12}$-3 | 31.7 | $g\left(LS \underset{264}{\overset{273}{\rightleftharpoons}} HS\right)\overset{303}{\rightarrow}Col_h\overset{456}{\rightarrow}d$ | 7.1 | 26.5 |

[a] The values correspond to the maxima of the peaks. Decomposition temperatures from the TGA data; g, glass; d, decomposition; Cr ($Cr_1$, $Cr_2$) crystalline; $Col_h$, columnar hexagonal; $Col_L$, columnar lamellar; LS, low spin, HS, high spin; [b] No SCO peak was observed on the cooling run. [c] The value on the second heating run. [d] The value on the first heating run.

main peaks (part c of Figure 1). The first intense one appearing without phase correction at 1.60 Å (i.e., 1.96 Å after correction, vide infra) can be attributed to the first $N_6$ coordination shell of the iron ion. The short distance clearly indicates the LS state. Also, several peaks are distinguishable in the region of 2−4 Å, which correspond to several kinds of distances such as Fe−N, Fe−C, and iron with its two nearest iron neighbors.[16] Particularly important is the weak intensity peak at ∼7.0 Å ascribed to the next-nearest iron neighbors of an Fe(II) ion in the chain. The presence of this peak is a clear demonstration of the polymer structure of $\mathbf{C}_{12}$-1.

From the EXAFS information, it is possible to conclude that the compound is indeed composed of triazole moieties building an octahedral coordination around the Fe(II) ions arranged in a 1D array, where the *N*1,*N*2 groups of triazole bridge adjacent metal centers.

The curve-fitting analysis for the first coordination sphere of the iron was performed (part d of Figure 1). The fitting variables were the distance Fe−N, the Debye−Waller factor $\sigma$, and the edge energy shift $\Delta E_0$. The coordination number $N$ was fixed to 6. The obtained values were $d^{Fe-N} = 1.96$ Å, $\sigma = 0.072$ Å, and $\Delta E_0 = -4.8$ eV with goodness of fit $\rho = 1.8\%$. The value of the Fe−N distance is in good agreement with that of the parent low spin compound $[Fe(tba)_3](CF_3SO_3)_2 \cdot 2H_2O$[15] and with previously reported data recorded on Fe(II) low-spin compounds.[18–22]

**X-ray Powder Diffraction (XRPD) for $\mathbf{C}_n$-1, $\mathbf{C}_n$-3, and Dynamic Light Scattering Data for $\mathbf{C}_{12}$-1 and $\mathbf{C}_{12}$-3.** The XRPD patterns of the compounds $\mathbf{C}_n$-1 with $n = 4$, 6 and $\mathbf{C}_n$-3 with $n = 4$, 6, 8, 10 were measured at 293 K. Variable temperature XRPD analysis was performed on compounds $\mathbf{C}_n$-1 with $n = 8$, 10, 12 and on $\mathbf{C}_{12}$-3. The derived structural parameter $d$ of compounds $\mathbf{C}_n$-1 and $\mathbf{C}_n$-3 at 293 K are presented in Table 1. For derivatives with $n =$ 4, 6, 8, the patterns are of poor quality, reflecting the low crystallinity of the samples (parts a, b, and c of Figure 2). Only two peaks are observed in the low- and high-angle regions. The hexagonal columnar ordering is deduced for compounds with $n = 10$, 12 from the intense peak (10) and minor peaks with the reciprocal distances at $1/3^{1/2}$ (11), $1/4^{1/2}$ (20), $1/7^{1/2}$ (21), and $1/9^{1/2}$ (30). The first one with the Miller indices $(hk) = (10)$ provides the stacking periodicity $d$ of the layers. The halo in the wide angle regime at $2\theta \sim 19°$ with spacing being 4.6 Å is assigned to the disordered alkyl chains. The lengthening of the alkyl substituent in the homologues with $n = 10$, 12 results into some ordering of the structure which is seen from the number of peaks in the low-angle region (parts d and e of Figure 2).

In $\mathbf{C}_8$-1, two other peaks are observed, the positions of which depend on temperature. In the pristine sample, one of the peaks is observed at $2\theta \sim 24.0°$, which after calculation gives a spacing of ∼3.70 Å. The peak is

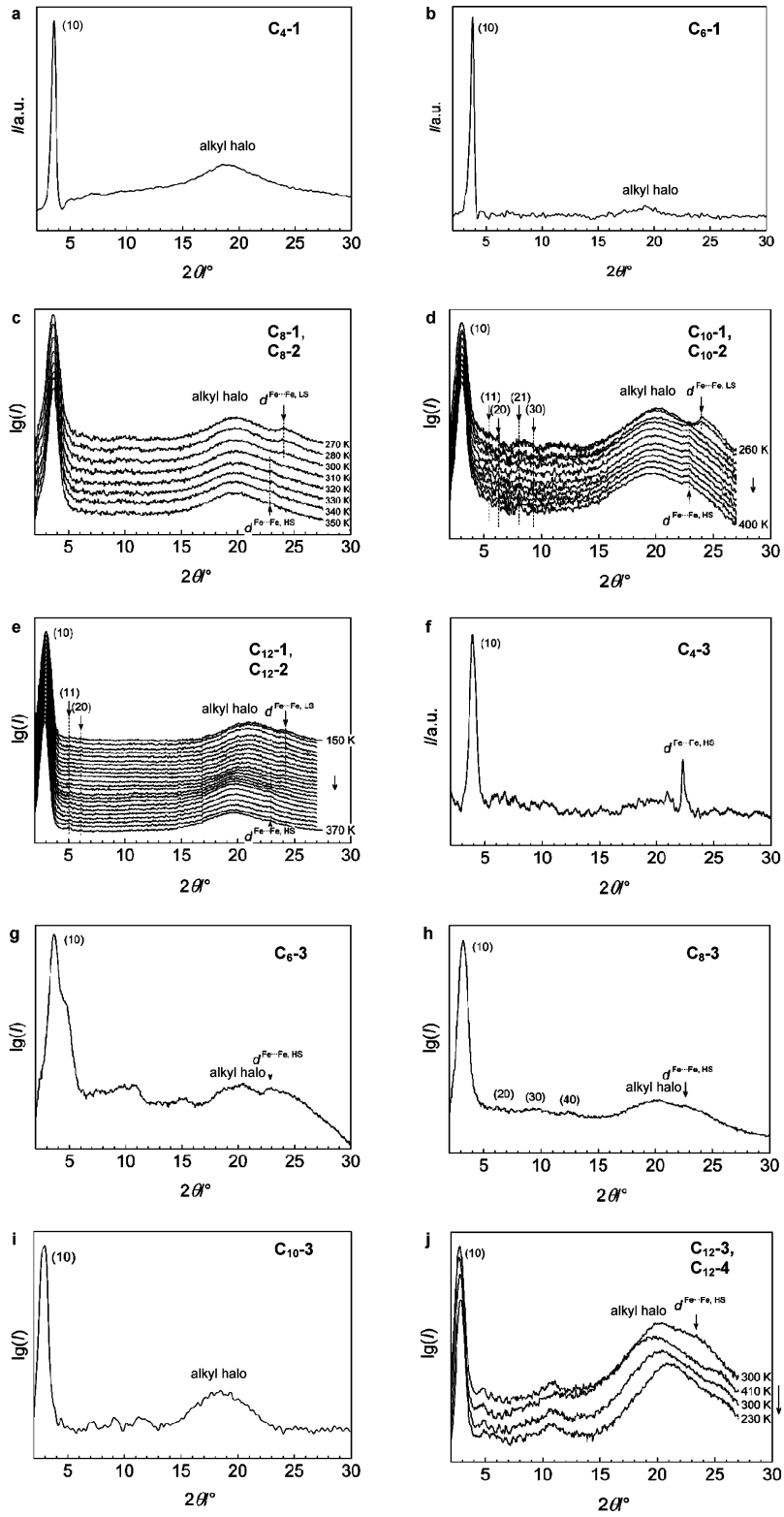


**Figure 2.** XRPD profiles for: a) $C_4$-1; b) $C_6$-1; c) $C_8$-1, $C_8$-2; d) $C_{10}$-1, $C_{10}$-2; e) $C_{12}$-1, $C_{12}$-2; f) $C_4$-3; g) $C_6$-3; h) $C_8$-3; i) $C_{10}$-3; j) $C_{12}$-3, $C_{12}$-4 measured at room temperature (for single profiles) or at temperatures indicated next to the profiles.

observable up to 300 K, but at 310 K it disappears. Instead, another peak appears at $2\theta \sim 22.9°$ with a spacing of ~3.90 Å. In $C_n$-1 with $n = 8$, 10, 12, the behavior of these peaks perfectly coincides with the spin transition as determined by the magnetic measurements (vide infra, in parts c−e of Figure 6). Accordingly, these peaks can be ascribed to the Fe···Fe separation, representing the distances along the main axis of the polymeric coordination chain. Because the coordination environment of the Fe(II) ion is spin state dependent and in the low-spin state Fe−N distances are shorter, at lower temperatures this results into shorter Fe···Fe spacing. In the high-spin state, the increase in the Fe−N distances moves neighboring Fe(II) ions apart. The precise value of the high spin

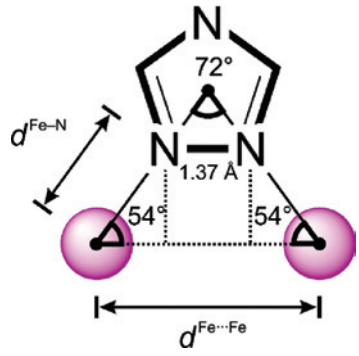


**Figure 3.** The simplified geometry of the triazole unit bridging two neighboring Fe(II) ions.

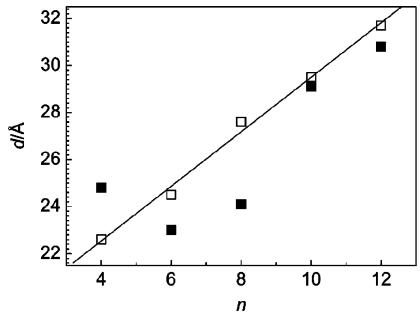


**Figure 4.** Dependence of interlayer distance $d$ on the length of alkyl chains $n$ in $\mathbf{C}_n$-1 (■) and $\mathbf{C}_n$-3 (□). The solid line represents the linear fit of the experimental points for $\mathbf{C}_n$-3.

Fe···Fe spacing can be measured in the high-spin trinuclear Fe(II)-based triazole complexes.[23] It is equal to 3.84 Å. The distance of 3.89 Å between neighboring copper(II) ions in the 1D polymer $[Cu(tba)_3](CF_3SO_3)_2 \cdot 3H_2O$[15] is also in agreement with the values found for the compounds $\mathbf{C}_n$-1 at higher temperatures. The observed Fe···Fe peak of the compounds $\mathbf{C}_n$-1 is reminiscent of the stacking peak observed in the XRPD profiles of the discotic liquid crystals, the molecules of which can stack into 1D columns with the regular periodicity defined by the nature of the material (3.5−3.8 Å).[24–26]

The model of the bridging by a triazole unit of two neighboring Fe(II) ions is illustrated in Figure 3. According to simple geometrical considerations the distance Fe−N ($d^{Fe-N}$) can be expressed through the spacing Fe···Fe ($d^{Fe\cdots Fe}$) by the equation

$$d^{Fe-N} = \frac{d^{Fe\cdots Fe} - 1.37}{2 \cos 54} \qquad (1)$$

where 1.37 is the distance in angstrom between bridging nitrogen atoms *N*1 and *N*2 of the triazole unit (CCDC, February 2008), the value 54° corresponds to the idealized mean angle Fe−Fe−N (Figure 3). The spacing Fe···Fe found at low temperature is 3.70 Å that gives a distance Fe−N equal to 1.98 Å. Above 300 K, the spacing increases up to 3.90 Å which corresponds to 2.15 Å of the Fe−N distance. Both calculated values are in rather good coincidence with the EXAFS data of the low-spin $\mathbf{C}_{12}$-1 and the reported EXAFS data on high-spin Fe(II)-based triazole complexes.[18–20]

Temperature-dependent 2D-WAXS patterns were recorded on the oriented sample of $\mathbf{C}_{12}$-1 ($\mathbf{C}_{12}$-2). The orientation was achieved by imposing the sample to mechanical stress. The 2D-WAXS patterns are similar at temperatures 150−390 K, which implies that the structure of the pristine $\mathbf{C}_{12}$-1 is also preserved in the anhydrous $\mathbf{C}_{12}$-2. The diffractogram recorded at 390 K is shown in SFigure 1 as a representative example. It consists of a pair of inner equatorial sharp peaks and a pair of meridional outer diffuse bands. The diffuse alkyl halo is situated in between. The analysis of these patterns confirms the columnar structure of the compound.

The nonlinear variation with temperature of the position of the alkyl peak was found only in compound $\mathbf{C}_{12}$-1. The width of the peak does not change on heating (part e of Figure 2), but the position of its maximum is temperature dependent. At low temperature, the peak gives a spacing of ∼4.2 Å, whereas upon heating from 240 up to 280 K it gradually increases with attaining the value of ∼4.5 Å, which is constant then up to 400 K. The phase transition influences the magnetic behavior and coincides in temperature with the magnetic hysteresis loop (vide infra, part e of Figure 6, upper right scale). In $\mathbf{C}_{10}$-1, the variation of the alkyl spacing has no evident discontinuity (200−400 K) being practically linear (vide infra, part d of Figure 6, upper right scale). In $\mathbf{C}_n$-1 with $n = 8, 10, 12$, the variation of the main peak (10) with temperature is negligible, showing only a minor linear increase on heating. In the case of $\mathbf{C}_{12}$-1, it is also insensitive to the variation of the alkyl peak.

The XRPD profiles of $\mathbf{C}_n$-3 are similar to those discussed just above. The poor crystallinity of the substances complicates the observation of the weak high-order peaks. As in the previous cases, the broad halo at $2\theta \sim 19°$ is due to liquid-like alkyl chains. In $\mathbf{C}_{12}$-3 like in the analogous $\mathbf{C}_{12}$-1, the broadness of the alkyl peak changes slightly on cooling, in addition to the shift of its maximum from $2\theta \sim 21°$ down to ∼19° (part j of Figure 2). The peak at $2\theta \sim 23°$ detected in the four compounds (parts f−h and j of Figure 2) is attributed to the spacing of Fe(II) HS ions along the polymeric chains. In $\mathbf{C}_{12}$-3, not all observed peaks were possible to index.

The reason for this is the poor ratio of noise/signal due to the almost amorphous nature of the substance. The final proof of the similar packing in compounds $\mathbf{C}_n$-3 was obtained on the basis of the interlayer distance $d$ plotted versus the length of alkyl substituents $n$ (Figure 4). As is seen, the dependence has a linear character, which points out a similar organization of the compounds. The effective size of the coordination core (the inner part of the polymeric chain without alkyl chains) in $\mathbf{C}_n$-3 can be determined from the fit of the experimental data (Figure 4). A linear regression of this plot ($R = 0.997$) gives a slope of 1.16 Å per $n$ and an intercept of 17.9 Å, which has to be near the size of the coordination core in parent $[Fe(tba)_3](BF_4)_2 \cdot 2H_2O$[15] (or $[Cu(tba)_3](CF_3SO_3)_2 \cdot$

(23) (a) Vos, G.; Le Febre, R. A.; De Graaff, R. A. G.; Haasnoot, J. G.; Reedijk, J. *J. Am. Chem. Soc.* **1983**, *105* (6), 1682. (b) Vos, G.; De Graaff, R. A. G.; Haasnoot, J. G.; Van der Kraan, A. M.; De Vaal, P.; Reedijk, J. *Inorg. Chem.* **1984**, *23*, 2905–2910. (c) Kolnaar, J. J. A.; van Dijk, G.; Kooijman, H.; Spek, A. L.; Ksenofontov, V. G.; Gütlich, P.; Haasnoot, J. G.; Reedijk, J. *Inorg. Chem.* **1997**, *36*, 2433–2440.

(24) Laschat, S.; Baro, A.; Steinke, N.; Giesselmann, F.; Hägele, C.; Scalia, G.; Judele, R.; Kapatsina, E.; Sauer, S.; Schreivogel, A.; Tosoni, M. *Angew. Chem., Int. Ed. Engl.* **2007**, *46*, 4832–4887.

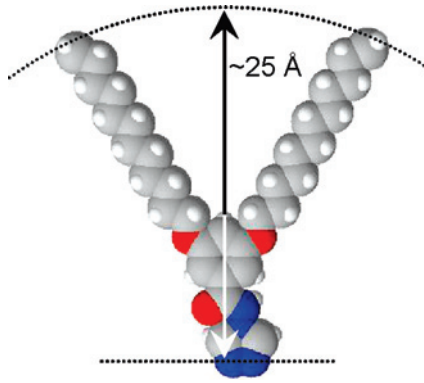


**Figure 5.** Molecular model of the ligand $C_{12}$−tba in the stretched configuration.

$3H_2O$), $n = 0$. Assuming that the packing is hexagonal, calculation using the formula $d^{cc} = (2/3^{1/2})dn = 0$ provides the diameter of the coordination core $d^{cc}$ to be 20.6 Å. The value obtained directly from the structure of $[Cu(tba)_3](CF_3SO_3)_2 \cdot 3H_2O$ is 19.7 Å. Indeed, both values are rather similar, and thus this confirms the validity of the proposed packing. The $d$ values of $\mathbf{C}_n$-1 are plotted in the same Figure 4. For the higher homologues, the dependence of the interlayer distances $d$ versus $n$ does not have a linear character but shows a discontinuity for $\mathbf{C}_6$-1 and $\mathbf{C}_8$-1, whereas the $d$ values of $\mathbf{C}_{10}$-1 and $\mathbf{C}_{12}$-1 lie near to the values of $\mathbf{C}_{10}$-3 and $\mathbf{C}_{12}$-3, respectively (Figure 4). Extrapolation to zero of the straight line drawn through the experimental points of $\mathbf{C}_6$-4 and $\mathbf{C}_8$-4 gives the value of $d^{n=0} = 19.7$ Å. It corresponds perfectly to the diameter of the coordination core in $[Cu(tba)_3](CF_3SO_3)_2 \cdot 3H_2O$. Accordingly, for these two homologues a lamellar packing of the polymeric chains is proposed.[27]

The molecular modeling of the ligand 3,5-bis(dodecyloxy)-*N*-(4*H*-1,2,4-triazol-4-yl)benzamide ($C_{12}$-tba) gives a distance of ca. 25 Å between the ends of the molecule in the stretched configuration (Figure 5). A radial arrangement of the ligand molecules in the polymeric chain would imply at least a twice larger diameter of the polymeric chain (~50 Å), which exceeds the experimentally observed one (for $\mathbf{C}_{12}$-3: $31.7 \times 2/3^{1/2} = 36.6$ Å). It can signify the tilt of the alkyl chains, for example, close to the axis of the polymeric chain. Taking also into account a possible interdigitation of the alkyl chains belonging to neighboring polymeric chains, one can explain the observed decrease of the effective diameter of the single polymeric chain.

The length of the polymeric chains in solution was evaluated by dynamic light scattering. For both $\mathbf{C}_{12}$-1 and $\mathbf{C}_{12}$-3, the averaged hydrodynamic radius of the polymeric species in chloroform is 780 Å. Assuming HS character of the Fe(II) ions, which is supported by the absence of coloration of the dissolved compounds, and taking into account an Fe···Fe distance equal to 3.9 Å, the approximate number or Fe(II) ions per chain is near to 400.

**Magnetic Properties of $\mathbf{C}_n$-1, $\mathbf{C}_n$-2, $\mathbf{C}_n$-3, and $\mathbf{C}_n$-4.** The magnetic properties of compounds $\mathbf{C}_n$-1 and $\mathbf{C}_n$-3 ($n = 4$, 6, 8, 10, 12) were measured in both cooling and heating modes to detect the influence of the temperature and dehydration on the magnetic properties of the compounds. The variation of the product of the molar magnetic susceptibility $\chi_M T$ versus temperature $T$ is shown in parts a−j of Figure 6. At room temperature, $\mathbf{C}_n$-1 are almost diamagnetic. The absence of the residual paramagnetism at low temperature is confirmed by Mössbauer measurements (vide infra) as well as by the closeness of the experimental $\chi_M T$ to the expected value for a pure singlet spin state (zero). The homologue $\mathbf{C}_4$-1 exhibits a spin transition centered near room temperature (part a of Figure 6). Subsequent cooling and heating reveals a narrow hysteresis loop ($\Delta T^{hys} \sim 3$ K), which disappears after heating up to 400 K. The thermal treatment of the complex was accompanied by the loss of half of a molecule of water (from TGA, STable 1 of the Supporting Information) and the transformation into anhydrous $\mathbf{C}_4$-2 with a spin transition centered at 226 K. As is seen in part a of Figure 6, at low temperature the fraction of the residual paramagnetic Fe(II) ions in the anhydrous compound increased. For $\mathbf{C}_n$-1 with $n = 6$, 8, 10, 12, the hysteresis in the pristine samples is no more observable (parts b−e of Figure 6). On the other hand, the temperature of the transition also increases (Figure 7). The influence of the water release is less pronounced for the higher homologues. Anhydrous $\mathbf{C}_{10}$-2 shows a narrow hysteresis loop detected with $\Delta T^{hys} \sim 2$ K (part d of Figure 6), whereas $\mathbf{C}_{12}$-2 has a complicated form of the loop with a characteristic feature at lower temperatures (near 275 K, part e of Figure 6). For $\mathbf{C}_{12}$-2, the incompleteness of the transition at higher temperatures is confirmed by the value of 3.14 $cm^3$ K $mol^{-1}$ attained at 350 K. However, for the homologues with shorter alkyl chains $\mathbf{C}_4$-2 and $\mathbf{C}_6$-2, the transition is assumed to be complete as confirmed by the susceptibility value equal to 3.50 $cm^3$ K $mol^{-1}$ at 350 K.

All compounds $\mathbf{C}_n$-3 are high-spin at room temperature (parts f−j of Figure 6). In $\mathbf{C}_4$-3, the transition is rather abrupt, being reminiscent of the parent compound $[Fe(tba)_3](BF_4)_2 \cdot 2H_2O$,[15] but $T_{1/2}$ is shifted by 30 K up to 270 K. The dehydration took place on heating up to 350 K, providing the anhydrous compound $\mathbf{C}_4$-4 with an incomplete gradual transition without hysteresis (part f of Figure 6). Despite the smoothing of the extremities of the transition, in compound $\mathbf{C}_6$-3 a narrow hysteresis is still observed ($\Delta T^{hys} = 4$ K). The dehydration completely changes the magnetic behavior making the spin transition gradual over the temperature range of 10−400 K (part g of Figure 6). In the three compounds $\mathbf{C}_n$-3 with $n = 8$, 10, 12, the magnetic behavior is somewhat similar. The pristine samples exhibit an incomplete spin transition with $T_{1/2} \sim 265$ K. On cooling, the transition is very gradual, leading to a substantial residual HS fraction at low temperatures (parts h−j of Figure 6). The decrease of the susceptibility below 40 K is due to zero field splitting. The anhydrous compounds $\mathbf{C}_n$-4 with $n = 8$, 10, and 12 obtained by heating of the pristine samples $\mathbf{C}_n$-3 up to 350 K or above are high spin and display only very moderate

(25) Glüsen, B.; Heitz, W.; Kettner, A.; Wendorff, J. H. *Liq. Cryst.* **1996**, *20*, 627–633.
(26) Binnemans, K.; Sleven, J.; De Feyter, S.; De Schryver, F. C.; Donnio, B.; Guillon, D. *Chem. Mater.* **2003**, *15*, 3930–3938.
(27) Kumar, S. *Chem. Soc. Rev.* **2006**, *35*, 83–109.

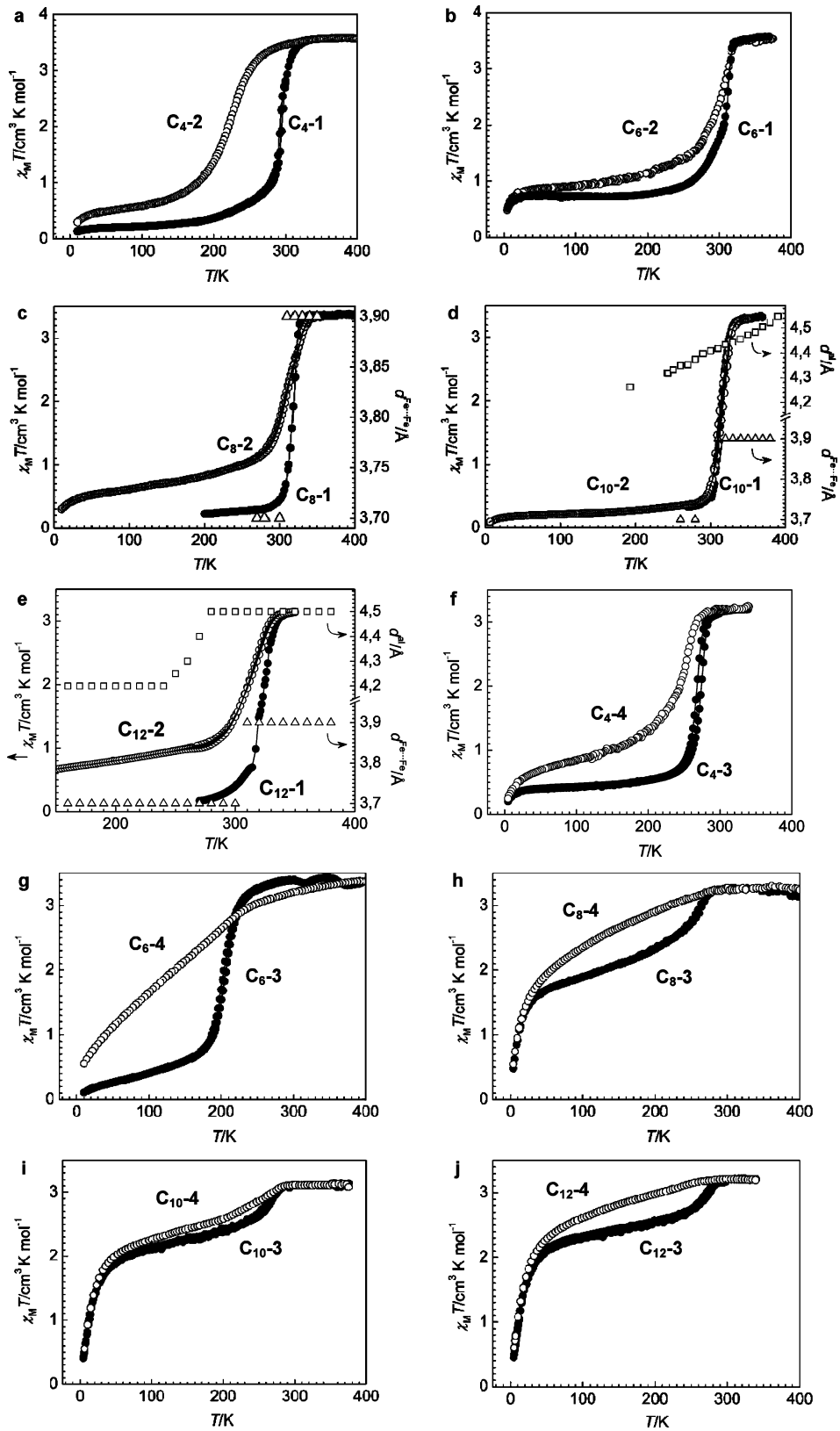


**Figure 6.** Plot of $\chi_M T$ vs $T$ for: a) $\mathbf{C}_4$-1 (●) and $\mathbf{C}_4$-2 (○); b) $\mathbf{C}_6$-1 (●) and $\mathbf{C}_6$-2 (○); c) $\mathbf{C}_8$-1 (●) and $\mathbf{C}_8$-2 (○). The value $d^{Fe\cdots Fe}$ (distance between neighboring Fe(II) ions in the polymeric chain) corresponds to compound $\mathbf{C}_8$-2; d) $\mathbf{C}_{10}$-1 (●) and $\mathbf{C}_{10}$-2 (○). The values $d^{alk}$ (of the alkyl halo) and $d^{Fe\cdots Fe}$ correspond to compound $\mathbf{C}_{10}$-2; e) $\mathbf{C}_{12}$-1 (●) and $\mathbf{C}_{12}$-2 (○). The values $d^{alk}$ and $d^{Fe\cdots Fe}$ correspond to compound $\mathbf{C}_{12}$-2; f) $\mathbf{C}_4$-3 (●) and $\mathbf{C}_4$-4 (○); g) $\mathbf{C}_6$-3 (●) and $\mathbf{C}_6$-4 (○); h) $\mathbf{C}_8$-3 (●) and $\mathbf{C}_8$-4 (○); i) $\mathbf{C}_{10}$-3 (●) and $\mathbf{C}_{10}$-4 (○); j) $\mathbf{C}_{12}$-3 (●) and $\mathbf{C}_{12}$-4 (○).

variation of the $\chi_M T$ on cooling (parts h−j of Figure 6). The value of $\chi_M T = 3.20$ cm$^3$ K mol$^{-1}$ attained by $\mathbf{C}_n$-4 in the high-temperature region corresponds to the incomplete transition with a partially preserved low-spin fraction. For comparison, Figure 7 displays the $T_{1/2}$ derived values plotted versus the length of alkyl chains $n$ for compounds $\mathbf{C}_n$-1, $\mathbf{C}_n$-

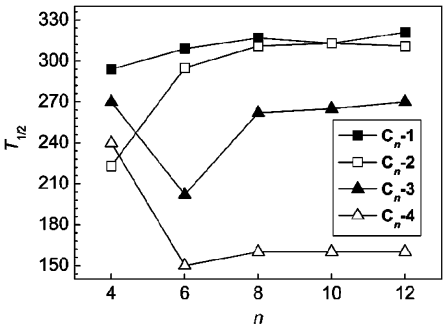


**Figure 7.** Plot of $T_{1/2}$ as a function of the value $n$ for $\mathbf{C}_n$-1, $\mathbf{C}_n$-2, $\mathbf{C}_n$-3, and $\mathbf{C}_n$-4.

2, $\mathbf{C}_n$-3, and $\mathbf{C}_n$-4. The spin transition in all compounds is accompanied by a drastic color change from violet (LS) to white (HS).

**Differential Scanning Calorimetry (DSC) and Polarizing Optical Microscopy (POM) Data of $\mathbf{C}_n$-1, $\mathbf{C}_n$-2, $\mathbf{C}_n$-3, and $\mathbf{C}_n$-4.** The spin and phase transitions in $\mathbf{C}_n$-1 and $\mathbf{C}_n$-3 were investigated using differential scanning calorimetry (DSC) (parts a−j of SFigure 2 in the Supporting Information). The first heating run for these compounds does not coincide with the second one as expected from the transformations, which undergo pristine samples upon heating above room temperature. For technical reasons, the DSC measurements were carried out with hermetically closed sample pans so that the results of the second cooling/heating run in most of the cases include the partial rehydration of the samples. One more reason for the rehydration or incomplete dehydration is the higher heating rate being 7 K $min^{-1}$, whereas, for example, the SQIUD experiments were done at 2 K $min^{-1}$. This means that the dynamic DSC measurements were less favorable for the equilibration of the systems, which underwent dynamic dehydration processes.

During the second measurement run, in $\mathbf{C}_n$-1 ($n = 4$, 6, 8, 10, 12) a heat capacity anomaly appears around 300 K, which corresponds to the spin transition observed by the magnetic measurements (parts a−e of SFigure 2 in the Supporting Information). Therefore, the heat capacity peaks obviously arise from the SCO phenomenon. The enthalpy $\Delta H^{SCO}$ deduced from the DSC data is about 15 kJ $mol^{-1}$, and the corresponding entropy $\Delta S^{SCO} \sim 47$ J $K^{-1}$ $mol^{-1}$ for the compounds $\mathbf{C}_n$-1 (Table 1). The entropy gain is larger than the value expected for the change of the spin manifold of an Fe(II) ion, vis. $R$ln5 (13.4 J $K^{-1}$ $mol^{-1}$), however, somewhat smaller than the corresponding values of the dehydrated parent compound $[Fe(tba)_3](CF_3SO_3)_2 \cdot 2H_2O$.[15] The difference arises from the incompleteness of the spin transition (parts a−e of Figure 6) and may furthermore be due to weaker cooperativity of the spin transition.[28] $\mathbf{C}_4$-1, $\mathbf{C}_6$-1, and $\mathbf{C}_8$-1 do not show any additional peaks that can be attributed to the phase transition of the alkyl chains (parts a, b, and c of SFigure 2 in the Supporting Information). For $\mathbf{C}_{10}$-1 and $\mathbf{C}_{12}$-1, a heat anomaly at 270 K was ascribed to the glass transition (parts d and e of SFigure 2 in the Supporting Information; Table 1).

The first heating/cooling cycle for $\mathbf{C}_4$-3 confirms the occurrence of an abrupt spin transition, which takes place just below room temperature (part f of Figure 6). A hysteresis loop with a width of 6 K was observed with transition temperatures, $T_c\uparrow = 261$ K and $T_c\downarrow = 255$ K in the heating and cooling modes, respectively. When compared to the SQUID magnetic data, the DSC thermograms reveal transitions over broader temperature ranges and are somewhat shifted relative to the value found from the magnetic data. We explain this by thermal conductivity of the materials, which becomes more important with the increase in the scanning rate. In $\mathbf{C}_6$-3 the spin transition peak is observed only partially because of the low-temperature limit of the utilized DSC facility (175 K). In $\mathbf{C}_4$-3 and $\mathbf{C}_6$-3, after the heating/cooling cycle the rehydration takes place, leading to the restoration of spin crossover properties (parts f and g of SFigure 2 in the Supporting Information) (for $\mathbf{C}_6$-3 is seen only the onset of the endothermic peak, part g of SFigure 2 in the Supporting Information, cooling run). Additional peaks observable in the cooling runs near 370 K for both compounds were tentatively attributed to solid−solid transitions and were not investigated in detail. For higher homologues with $n = 8$, 10, 12, the change of the magnetic properties, that is, shift of the spin transition to about 270 K and its incomplete character are reflected in the character of the anomalies detected by DSC (parts h−j of SFigure 2 in the Supporting Information). Additionally, in the compounds $\mathbf{C}_{10}$-3 and $\mathbf{C}_{12}$-3 a broad peak of low energy indicating minor structural changes are found, which may be attributed to the vitrification of the samples ($T_g \sim 300$ K). The second heating run for these compounds shows the same behavior pointing out rehydration under the sealed conditions.

The examination of the anisotropic textures by polarized optical microscopy (POM) showed that $\mathbf{C}_n$-1 and $\mathbf{C}_n$-3 ($\mathbf{C}_n$-2 and $\mathbf{C}_n$-4) with $n = 8$, 10, 12 form a liquid crystal. For $\mathbf{C}_n$-1 upon heating at ca. 310 K, the coloration of the samples changed from purple to colorless due to the spin transition LS → HS. Despite high viscosity, the flow could nevertheless be induced by pressing the coverslip with a needle. On further heating, the mesophase persisted up to 450 K; however, the viscosity was found to decrease greatly. No decomposition or clearing due to isotropization was observed at this temperature. On cooling, the viscosity gradually increased, and the mesophase could still be observed at room temperature. For $\mathbf{C}_n$-1 ($\mathbf{C}_n$-2), the purple coloration was recovered at about 300 K. Derived parameters for $\mathbf{C}_n$-1 and $\mathbf{C}_n$-3 are collected in Table 1.

**Mössbauer Spectroscopy of $\mathbf{C}_n$-1, $\mathbf{C}_n$-3, and $\mathbf{C}_{12}$-4.** $^{57}$Fe Mössbauer spectra of compounds $\mathbf{C}_n$-1 and $\mathbf{C}_n$-3 ($n = 4$, 6, 8, 10, 12) were recorded between 4.2 and 340 K (parts a−k of SFigure 3 in the Supporting Information). The parameters derived from least-squares fitting are listed in STable 2 in the Supporting Information. The observed spectra could be fitted considering LS and HS asymmetric doublets with a ratio of area fractions in agreement with the magnetic data.

(28) Kröber, J.; Audière, R.; Claude, R.; Codjovi, E.; Kahn, O.; Haasnoot, J. G.; Crolière, F.; Jay, C.; Bousseksou, A.; Linares, J.; Varret, F.; Gonthier-Vassal, A. *Chem. Mater.* **1994**, *6*, 1404–1412.

The large quadrupole splittings observed for the HS doublets of $\mathbf{C}_n$-1, $\mathbf{C}_n$-3, and $\mathbf{C}_{12}$-4 (Table 2) can arise from a noncubic valence electron distribution over the iron molecular orbitals. This can be the result of axial distortion for $d^6$ complex ions in the degenerated $^5T_{2g}$ ground state. For the electric quadrupole splitting to be observed for an Fe(II) HS complex, the octahedral distortion should be such that a splitting of the $t_{2g}$ orbital subset occurs on the order of a few hundred wavenumbers. The value calculated for $\mathbf{C}_4$-1 according to the equation

$$\frac{\Delta E_Q(T)}{\Delta E_Q(0)} = \frac{1 - e^{-\frac{E_0}{k_B T}}}{1 + 2e^{-\frac{E_0}{k_B T}}} \qquad (2)$$

is ca. 530 $cm^{-1}$. The large quadrupole splittings $\Delta E_Q$ can be observed for pseudo-octahedral Fe(II) HS compounds in cases where the doubly occupied $d_{xy}$ orbital lies lowest. This corresponds to octahedral compression. The additional factor is the lattice contribution which, however, is relatively small and decreases the valence contribution.

The rather pronounced residual HS fraction in $\mathbf{C}_8$-3, $\mathbf{C}_{10}$-3, and $\mathbf{C}_{12}$-3 deduced from the magnetic data raises the question about its nature. Two explanations can be proposed: (i) The compounds have a polymeric structure but suffer from defects of coordination. Therefore, not all Fe(II) ions are surrounded by six nitrogen atoms, but there is a substantial fraction having the $N_4O_2$ coordination environment; (ii) an incomplete transition is the feature of the essentially polymeric compound because of, for example, imperfect packing of the polymeric chains. An analogy can be drawn with the magnetic properties of powdered spin crossover crystalline systems that are affected by the defects in the crystal lattice, which flattens the transition curve and increases the residual HS fraction at low temperature.[1] These two cases can be distinguished by the Mössbauer data, assuming that Fe(II)-based species with different coordination environments should have different quadrupole splittings $\Delta E_Q$. Comparing the derived values of the quadrupole splitting for $\mathbf{C}_8$-3, $\mathbf{C}_{10}$-3, and $\mathbf{C}_{12}$-3 (3.31, 3.28, and 3.28 mm $s^{-1}$, respectively) with the corresponding value of the genuine spin crossover $\mathbf{C}_6$-3 (3.27 mm $s^{-1}$) one can find that all values are very similar. The Mössbauer spectrum of the dehydrated compound $\mathbf{C}_{12}$-3 (i.e., of $\mathbf{C}_{12}$-4) did not reveal appearance of a new HS doublet because fitting with one HS doublet gave satisfactory results (part k of SFigure 3 in the Supporting Information). The only observed change is the relative increase of the high-spin fraction at the expense of the low-spin fraction, which is expected from the magnetic data (part j of SFigure 6 in the Supporting Information). Consequently, the conclusion was made about the polymeric nature of $\mathbf{C}_{12}$-3 and its dehydrate $\mathbf{C}_{12}$-4 where each Fe(II) ion is connected to the neighboring Fe(II) ions through three triazole bridges adopting an $N_6$ coordination environment. The conclusion is supported by the CHN analysis, IR, and dynamic light scattering data.

As was proposed in several reports, the averaged length of polymeric chains could be evaluated from the Mössbauer or magnetic data at low temperature by the assumption that the high-spin fraction under this condition originates exclusively from the terminal iron ions with the $Fe^{II}N_3O_3$ chromophore with three oxygen atoms belonging to capping water molecules: $N = 2\ (100/\gamma_{HS})$ or $N = 2(\chi_M T_{\text{high temp}}/\chi_M T_{\text{low temp}})$.[29] For example, for $\mathbf{C}_{12}$-1 this gives only 26 Fe(II) ions per one chain that is strongly underestimated in comparison with the light scattering data (400). This again implies the necessity to consider imperfections of the lattice, which favors the HS state even by those Fe(II) ions that are surrounded by nitrogen atoms of the triazole units.

**Preparation of $\mathbf{C}_n$-1, $\mathbf{C}_n$-2, and $\mathbf{C}_n$-3 ($n$ = 8, 10, 12) as Thin Films.** An interesting and important feature is the possibility to obtain these materials in the form of thin films. Around 10 mg of $\mathbf{C}_n$-1 and $\mathbf{C}_n$-3 complexes were dissolved in $CHCl_3$ (1 mL), and subsequently the solution was layered onto a glass plate and allowed the solvent to evaporate. Thin films of a few micrometers thick form after solvent evaporation. A reversible change between the violet (LS state) and white (HS state) coloration of the films by heating or cooling around 300 K was observed without fatigue. $\mathbf{C}_n$-2 can be prepared as thin films by heating $\mathbf{C}_n$-1 films up to 330 K under ambient conditions. The water reabsorption process has been investigated and shows that the compounds reabsorb the water molecules in an open atmosphere within 10 days; however, this does not influence much the thermochromic properties (cf. parts c−e of Figure 6).

## Discussion

Before discussing the correlation between structure and magnetic properties in $\mathbf{C}_n$-1 and $\mathbf{C}_n$-3 ($n$ = 4, 6, 8, 10, 12) we shall clarify why the compounds under discussion can be considered as chain-like polymeric materials. The linear structure of the nonalkylated parent compound $[Fe(tba)_3](CF_3SO_3)_2 \cdot 2H_2O$ was established unambiguously on the basis of the EXAFS data supported also by the crystal structure analysis of the analogous triazole-based copper(II) polymer $[Cu(tba)_3](CF_3SO_3)_2 \cdot 3H_2O$.[15] Support for the polymeric structure of the compound $[Fe(tba)_3](BF_4)_2 \cdot 2H_2O$ comes from the IR data along with the Mössbauer and magnetic data. The alkylation of the parent systems $[Fe(tba)_3](CF_3SO_3)_2 \cdot 2H_2O$ and $[Fe(tba)_3](BF_4)_2 \cdot 2H_2O$ resulted in the formation of $\mathbf{C}_n$-1 and $\mathbf{C}_n$-3. The EXAFS data of the $\mathbf{C}_{12}$-1 confirm the polymeric structure in close analogy with the parent system $[Fe(tba)_3](CF_3SO_3)_2 \cdot 2H_2O$. Furthermore, IR spectroscopic study carried out on the alkylated materials shows that the triazole units retain $C_{2v}$ symmetry, disclosing the *N*1,*N*2-bridging coordination mode of the triazole units. For $\mathbf{C}_n$-1, the small amount of remaining paramagnetism at low temperature indicates that most of the Fe(II) ions undergo a thermal spin transition, which in turn points at the $N_6$ surroundings for most of the Fe(II) ions. However, the incomplete spin transition at low temperatures for $\mathbf{C}_n$-3 with $n$ = 8, 10, 12 raises the question about its nature. Earlier, several authors proposed the trinuclear structure for the alkylated triazole-based compounds with an incomplete

(29) Fujigaya, T.; Jiang, D. L.; Aida, T. *J. Am. Chem. Soc.* **2005**, *127*, 5484–5489.

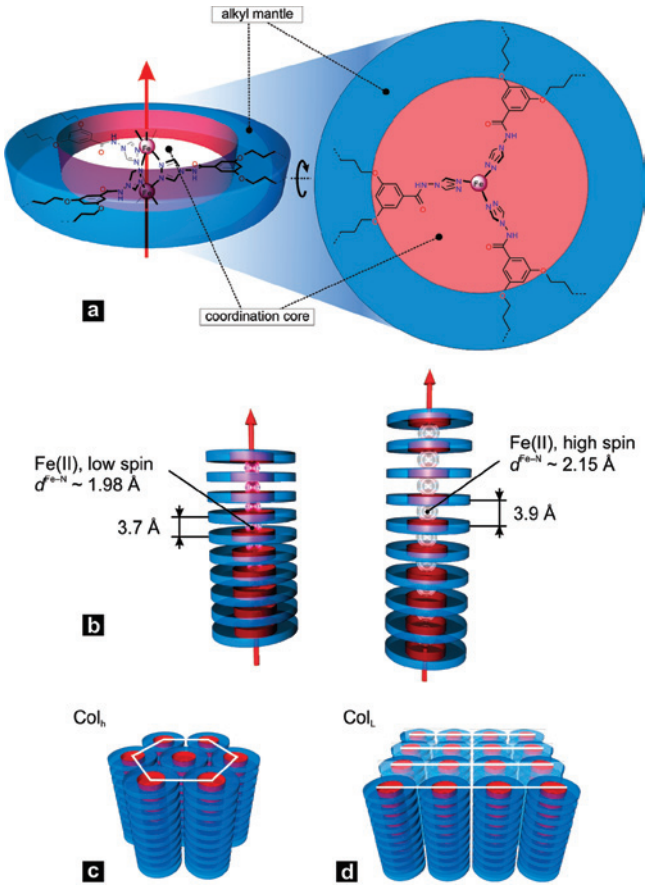


**Figure 8.** a) Schematic ideal structure of the monomeric unit in $\mathbf{C}_n$-1 and $\mathbf{C}_n$-3 (a neighboring Fe(II) ion is added for clarity). The inner part of the chain is the coordination core made by the linearly arranged Fe(II) ions bridged by three triazole moieties (pink). The coordination core is surrounded by the covalently tethered alkyl chains in the peripheral part (blue); b) polymeric chains in the LS state (left) and HS state (right). The distances are defined by the Fe−N bond lengths (larger for HS than for LS); c) hexagonal columnar packing $Col_h$ of the polymeric chains in $\mathbf{C}_n$-1 and $\mathbf{C}_n$-3 except $\mathbf{C}_6$-1 and $\mathbf{C}_8$-1; and d) Lamellar columnar packing $Col_L$ of the polymeric chains in $\mathbf{C}_6$-1 and $\mathbf{C}_8$-1.

transition.[30,31] We have checked this hypothesis on these compounds with the dynamic light scattering technique and Mössbauer spectroscopy. The obtained results show that the polymeric structure is adopted by all compounds $\mathbf{C}_n$-3 independently of $n$. The incomplete spin transition is rather a special feature of the compounds and probably arises from imperfections of the packing in these soft materials. This spin transition behavior was already observed in anhydrous derivatives $[Fe(C_n\text{-tba})_3](4\text{-}MeC_6H_4SO_3)_2$ with $n = 8$, 10, 12.[12a,b]

The higher homologues of the series $\mathbf{C}_n$-1 and $\mathbf{C}_n$-3 with $n = 8$, 10, 12 exhibit the columnar mesomorphism. According to the XRPD data of $\mathbf{C}_8$-1, a columnar lamellar mesophase ($Col_L$) can be ascribed to this compound while the rest of the higher homologues possesses hexagonal packing of the polymer chains adopting the hexagonal columnar mesophase $Col_h$. In Figure 8 is shown the structure of the polymeric chains along with the spin-state dependent intra-chain Fe···Fe periodicity and two packing motifs of the polymeric chains in the mesophase, $Col_h$ and $Col_L$.

On lengthening the alkyl chains, the magnetic properties of $\mathbf{C}_n$-1 and $\mathbf{C}_n$-3 change from those typical for crystalline spin crossover compounds ($n = 4$, 6) to those that coexist with the liquid crystalline properties ($n = 8$, 10, 12). It was found that the pristine compounds are hydrates which lose solvate water on heating and generate new anhydrous compounds $\mathbf{C}_n$-2 and $\mathbf{C}_n$-4. Both forms differ in their spin transition characteristics; however, the difference between the pristine and the dehydrated compounds depends on the type of the anion. For the triflate ($CF_3SO_3^-$) compounds $\mathbf{C}_n$-1 and $\mathbf{C}_n$-2, the magnetic properties of both forms are quite similar (parts a−e of Figure 6), whereas for the tetrafluoroborate ($BF_4^-$) compounds $\mathbf{C}_n$-3 the heating provokes the dehydration to yield $\mathbf{C}_n$-4, which changes the character of the spin transition to a very gradual one (parts f−j of Figure 6).

In the following, we shall discuss the role of the structural variables that have influence on the magnetic properties of the compounds, namely: i) the type of the anion ($CF_3SO_3^-$ or $BF_4^-$) and the water content of the compound; ii) the length of alkyl chains and the role of the glass transition and of the mesophase. One more factor that could influence the magnetic properties is the packing of polymeric polymeric chains, but it is apparently unimportant as follows from the practically similar magnetic data of $\mathbf{C}_8$-1 and $\mathbf{C}_{10}$-1, which adopt lamellar and hexagonal packing, respectively.

**Anion and Water Content.** The role of the noncoordinated solvent molecules in most Fe(II) spin crossover complexes is well understood. The incorporation of the solvent molecules into the crystal lattice mostly influences the interlinking of the spin crossover centers and leads to higher transition temperatures and abruptness of the spin transition. An early example was provided by the compounds $[Fe(2\text{-pic})_3]Cl_2 \cdot s$Solv, where Solv = $C_2H_5OH$ or $CH_3OH$, or $H_2O$, or $2H_2O$.[32] The spin transition temperature was found to increase along the series, which was assigned to the nature of the solvent molecules.[33,34] Specific hydrogen bonding of lattice water molecules was also noticed. As it was discussed in ref 35, the explanation of the hydrogen bonding effect and its influence on the parameter $T_{1/2}$ implies formation of the strong hydrogen bonds N−H···$OH_2$, where the nitrogen atom belongs to the heterocycle or amine group directly bonded to the Fe(II) ion. This interaction results in strengthening the metal−ligand interaction and then favoring the low-spin state at higher temperatures.[36,37] In contrast, the N···H−OH interaction, where nitrogen is the imine

(30) Roubeau, O.; Gomez, J. M. A.; Balskus, E.; Kolnaar, J. J. A.; Haasnoot, J. G.; Reedijk, J. *New J. Chem.* **2001**, *25*, 144–150.
(31) Armand, F.; Badoux, C.; Bonville, P.; Ruaudel-Teixier, A.; Kahn, O. *Langmuir* **1995**, *11*, 3467–3472.
(32) Sorai, M.; Ensling, J.; Hasselbach, K. M.; Gütlich, P. *Chem. Phys.* **1977**, *20*, 197–208.
(33) Gütlich, P.; Köppen, H.; Steinhäuser, H. G. *Chem. Phys. Lett.* **1980**, *74*, 475–480.
(34) Hostettler, M.; Tornroos, K. W.; Chernyshov, D.; Vangdal, B.; Burgi, H. B. *Angew. Chem., Int. Ed.* **2004**, *43*, 4589–4594.
(35) Garcia, Y.; van Koningsbruggen, P. J.; Lapouyade, R.; Fournes, L.; Rabardel, L.; Kahn, O.; Ksenofontov, V.; Levchenko, G.; Gütlich, P. *Chem. Mater.* **1998**, *10*, 2426–2433.
(36) Toftlund, H.; McGarvey, J. J. In *Spin Crossover in Transition Metal Compounds I* **2004**, *Vol. 233*, 151–166.
(37) Leita, B. A.; Moubaraki, B.; Murray, K. S.; Smith, J. P.; Cashion, J. D. *Chem. Commun.* **2004**, 156–157.

nitrogen atom, favors the stabilization of the high spin state. In this case, $T_{1/2}$ is shifted toward lower temperatures in comparison to the anhydrous compound. $\mathbf{C}_n$-1 and $\mathbf{C}_n$-3 possess no free imine groups; they only have amide groups. However, as follows from the magnetic data, the nitrogen atom seems to be not involved in the hydrogen bonding with the water molecule. Therefore, the observed change in the magnetic properties on dehydration cannot be attributed to an electronic effect induced by the kinds of hydrogen bonding discussed above.

In the particular case of the triazole complexes, the role of water is assumed to be important as stated in numerous reports[22,28,30,38–40] and was also noticed in alkylated compounds $[Fe(C_n\text{-tba})_3](4\text{-}MeC_6H_4SO_3)_2 \cdot H_2O$.[12a,b] However, to the best of our knowledge the involvement of water molecules into the crystal lattice of the triazole-based Fe(II) polymers was never analyzed despite available crystal structures of the copper(II) analogues. According to the crystal data, in $[Cu(tba)_3](CF_3SO_3)_2 \cdot 3H_2O$[15] and $[Cu(NH_2\text{-}trz)_3](BF_4)_2 \cdot H_2O$[40] the water molecules bridge CH groups of the neighboring triazole units reinforcing the polymeric chain by weak double hydrogen bonds CH···Ow···HC (part a of SFigure 4 in the Supporting Information). In the case where the number of water molecules per monomeric unit is less than three, the anion is involved in the double hydrogen bonding with the CH groups of the triazole rings (parts b and c of SFigure 4 in the Supporting Information). It seems also to be the case for the parent compound $[Fe(tba)_3](CF_3SO_3)_2 \cdot 2H_2O$,[15] which has two molecules of water in the pristine form. Comparison of the polymers $[Cu(hyettrz)_3](CF_3SO_3)_2 \cdot H_2O$ (hyettrz = 4-(2′-hydroxy-ethyl)-1,2,4-triazole)[41] (part b of SFigure 4 in the Supporting Information) and $[Cu(NH_2trz)_3](BF_4)_2 \cdot H_2O$[40] (part c of SFigure 4 in the Supporting Information) does not show any differences between the involvement of the anions $BF_4^-$ and $CF_3SO_3^-$ in the weak hydrogen bonding. In both cases, the anions bridge the neighboring triazole moieties through the oxygen atom or the fluorine atom, as is depicted in parts b and c of SFigure 4 in the Supporting Information. Because both types of the anions can be involved in the hydrogen bonding with the triazole units, the higher transition temperatures of the reported triflate-based compounds probably originate from a larger electrostatic pressure created by this type of anion.[42] The properties exhibited by the parent compounds $[Fe(tba)_3](CF_3SO_3)_2 \cdot 2H_2O$ and $[Fe(tba)_3](BF_4)_2 \cdot 2H_2O$ can be explained in a similar way.

The same explanation is also valid for the alkylated Fe(II) derivatives. The TGA data show that $\mathbf{C}_n$-1 contain only half a molecule of water per monomeric unit, which means also that the oxygen atoms of the triflate anions might be involved in the hydrogen bonding of the triazole units (part b of SFigure 4 in the Supporting Information), which can explain the observed abrupt spin transition in anhydrous $\mathbf{C}_n$-2 (and also in the parent $[Fe(tba)_3](CF_3SO_3)_2$) (parts a−e of Figure 6). On the other hand, for the $BF_4^-$ derivates the loss of the lattice water molecules drastically decreases the cooperativity, resulting in a very gradual incomplete spin transition in $[Fe(tba)_3](BF_4)_2$ and $\mathbf{C}_n$-4, which can imply that the hydrogen bridging of the triazole units through the $BF_4^-$ anions (like that shown in part c of SFigure 4 in the Supporting Information) is not so effective or not realized at all. The IR data in the region of the absorption band B−F confirm the decrease of the symmetry of the tetrafluoroborate anions because of the interaction with the lattice surrounding that might indicate the involvement in the hydrogen bonding.

**Alkyl Chains and Phase Transition.** By introducing alkyl substituents into the ligand *tba*, the separation between the neighboring polymeric chains was increased (Figure 4). The resulting effect on the magnetic properties depends on the length of the substituents (parts a−j in Figure 6 and Figure 7). If we consider the 3D character of the intermolecular contacts in the parent compounds $[Fe(tba)_3](CF_3SO_3)_2 \cdot 2H_2O$ and $[Fe(tba)_3](BF_4)_2 \cdot 2H_2O$, the interactions in the derivatives $\mathbf{C}_n$-1 and $\mathbf{C}_n$-3 become a 1D character; consequently, this should diminish the hysteresis or the steepness of the spin transition.[31] Indeed, in comparison with the parent complexes, the $T_{1/2}$ changes slightly being ∼300 K but, for example, in $\mathbf{C}_4$-1 and $\mathbf{C}_6$-1 the width of the hysteresis loop is reduced. Because the parent and alkylated derivatives differ from each other only by the alkyl substituent on the triazole ligands, this result tends to show that in the unalkylated polymers there is the interchain contribution to the overall cooperativity of the spin transition, which correlates with the conclusions of other researchers.[30,31] Lengthening the alkyl chains influences the $T_{1/2}$ value in a rather gradual way for both the pristine and the dehydrated compounds as shown in Figure 7. With the triflate anion, one can observe a monotonic increase of $T_{1/2}$ with $n$, whereas for the tetrafluoroborate compounds the dependence has a complicate character, but for the higher homologues the increase is apparent as well. In general, an increase of $n$ decreases the completeness of the spin transition in both low- and high-temperature regions.

Roubeau et al.[30] reported on the absence of the general dependence of the magnetic properties on the length of the alkyl chain in the systems formed by 4-*n*-alkyl-triazoles. However, their report covered only part of the alkylated systems because of encountered synthesis problems.[30] Kojima et al. reported on the triazole systems with alkylated anion of the general formula $[Fe(NH_2trz)_3](C_mH_{2m+1}SO_3)_2 \cdot 2H_2O$ ($m = 1-9$), where a gradual dependence of the $T_{1/2}$ parameter on $m$ was found.[43] From EXAFS measurements, it was apparent that the distance Fe···Fe within the polymeric chains decreases with increasing $m$, which was supposed to be induced by the fastener effect of the alkyl chains. In the

(38) Kröber, J.; Codjovi, E.; Kahn, O.; Groliere, F.; Jay, C. *J. Am. Chem. Soc.* **1993**, *115*, 9810–9811.
(39) Roubeau, O.; Haasnoot, J. G.; Codjovi, E.; Varret, F.; Reedijk, J. *Chem. Mater.* **2002**, *14*, 2559–2566.
(40) Drabent, K.; Ciunik, Z. *Chem. Commun.* **2001**, 1254–1255.
(41) Garcia, Y.; van Koningsbruggen, P. J.; Bravic, G.; Chasseau, D.; Kahn, O. *Eur. J. Inorg. Chem.* **2003**, 356–362.
(42) Garcia, Y.; van Koningsbruggen, P. J.; Bravic, G.; Chasseau, D.; Kahn, O. *Eur. J. Inorg. Chem.* **2003**, 356–362.
(43) Kojima, N.; Toyazaki, S.; Itoi, M.; Ono, Y.; Aoki, W.; Kobayashi, Y.; Seto, M.; Yokoyama, T. *Mol. Cryst. Liq. Cryst.* **2002**, *376*, 567–574.

case of $\mathbf{C}_n$-1 and $\mathbf{C}_n$-3 where the coordination core is surrounded by the mantle of the covalently tethered alkyl chains (part a of Figure 8) the same effect can be called for the explanation of the observed increase of $T_{1/2}$ with $n$.

For the triflate-based anhydrous compounds, $\mathbf{C}_n$-2 reappearance of the magnetic hysteresis loop in the homologues with $n = 8$, 10, 12 can by no means be attributed to the increase of the interchain cooperativity. The explanation should be looked for in the fact that those compounds down to 270 K are in the liquid-crystalline state as was determined by XRPD, DSC, and POM measurements. The width of the loop is quite small ($\Delta T^{hys} \sim 2$ K), which points out that upon spin transition the liquid crystalline compounds exhibit relatively small structural reorganization. Additionally, the complicate form of the loop for $\mathbf{C}_{12}$-2 shows an influence of the glass transition on the magnetic properties. The feature detected at the low-temperature edge near 275 K coincides with the anomaly detected by the XRPD and DSC techniques.

As discussed in the literature,[30,44,45] the interchain interactions in triazole-based spin crossover polymers are important for defining the abruptness and hysteresis of the spin transition. However, as we have shown in this work, in the alkylated system upon passing some threshold of the chain length a new effect comes into play, which modifies the characteristics of the spin transition. This effect is liquid crystallinity. The semifluid nature of the liquid-crystalline materials is responsible for the delay effect in the restoring of the magnetic properties upon subsequent heating/cooling.

In summary, we have presented novel metallomesogens exhibiting liquid crystalline properties and spin-state transition in the room-temperature region. The compounds investigated represent new examples of systems of type ib) where the phase transition (mesophase) directly influences the spin state change of the Fe(II) ions but it is not the driving force of the spin crossover phenomenon. The compounds display drastic changes of color from violet (low-spin state, LS) to white (high-spin state, HS). By the virtue of their fluid nature, it is possible to prepare the compounds as thin films.

## Experimental Section

**Physical Measurements.** Variable-temperature magnetic susceptibility measurements of samples $\mathbf{C}_n$-1, $\mathbf{C}_n$-2, $\mathbf{C}_n$-3, and $\mathbf{C}_n$-2 (20−30 mg) were recorded with a Quantum Design MPMS2 SQUID susceptometer equipped with a 7 T magnet, operating at 1 T and at temperatures from 1.8−400 K. The susceptometer was calibrated with $(NH_4)_2Mn(SO_4)_2 \cdot 12H_2O$. Experimental susceptibilities were corrected for diamagnetism of the constituent atoms by the use of Pascal's constants. Mössbauer spectra were recorded in transmission geometry with a $^{57}$Co/Rh source kept at room temperature and a conventional spectrometer operating in the constant-acceleration mode. The samples were sealed in a Plexiglass sample holder and mounted in a nitrogen-bath cryostat. The Recoil 1.03a Mössbauer Analysis Software (Dr. E. Lagarec; http://www.isapps.ca/recoil/) was used to fit the experimental spectra. DSC measurements were performed on a Mettler model DSC 822e calibrated with metallic indium and zinc. DSC profiles were recorded at the rate of 10 K/min and analyzed with *Netzsch Proteus* software (NETZSCH-Geraetebau GMBH, http://www.e-thermal.com/proteus.htm). An overall accuracy of 0.2 K was estimated in the temperature control and 2% in the heat flow. X-ray measurements were obtained with a Seifert TT3300 diffractometer (monochromatic Cu K$\alpha$ radiation). The 2D WAXD data were obtained by means of wide-angle X-ray diffraction (WAXD) (Bruker GADDS) in the range of $2\theta = 2-30°$. The temperatures and textures of phase transitions were determined with a polarization microscope, equipped with a hot stage and with temperature control of better than ± 0.5 K. IR spectra were recorded at 293 K using a Bruker Tensor 27 Spectrometer in the range of 400−4000 cm$^{-1}$. Elemental analyses were done on a Vario EL Mikro Elementaranalysator. $^1$H NMR spectroscopic measurements were done on an Advance DRX Bruker 400 MHz Spectrometer. TGA measurements were performed on a Mettler Toledo TGA/SDTA 851, in the 300−680 K temperature range in nitrogen atmosphere with a rate of 10 K/min. Dynamic light scattering (DLS) was performed with an argon ion laser (Stabilite 2060−04, $\lambda$ 514 nm, Spectra-Physics), a SP-125 goniometer, and an ALV-5000 multiple-tau digital correlator. The temperature was kept constant at 293 K for light-scattering measurements. The concentration of the analyzed substance was 1 mmol/L and 2 mmol/L.

**X-ray Absorption Data Recording and Processing.** The iron K-edge XANES (X-ray absorption near-edge structures) and EXAFS (extended X-ray absorption fine structures) spectra were recorded in the conventional transmission mode on beamline A1 at the German Electron Synchrotron, DESY, Hamburg. The spectrum was recorded from 6970 to 7997 eV. The energy scale at the iron K-edge was calibrated with the strong absorption peak of metallic iron foil at 7111.2 eV. A water-cooled Si(111) channel-cut crystal was used as a monochromator. The intensities of the incident and transmitted X-rays were recorded using ionization chambers. The mass of the sample was calculated to obtain a product $a \times d$ of about 2.5 for energies just above the absorption K-edge of iron ($a$ is the linear absorption coefficient and $d$ is the thickness of the pellet). The calculated amount of the sample was ground, mixed with crystalline cellulose, and pressed into a 13 mm diameter and about 1 mm thick pellet. The temperature of the experiment was 80 K. For this purpose, a closed-cycle helium cryostat was used, and the temperature was measured with a silicon diode placed close to the sample. The data acquisition time for each data point was 1 s. EXAFS data analysis was performed with the program *EXAFS98*.[46] This standard analysis includes linear pre-edge background removal, a Lengeler−Eisenberg spectrum normalization, and reduction from the absorption data $\mu(E)$ to the EXAFS spectrum $\chi(k)$ with

$$k = \sqrt{\frac{2m_\varepsilon}{(\hbar)^2}(E - E_0)} \qquad (3)$$

where $E_0$ is the energy threshold, taken at the absorption maximum (7130 ± 1 eV). The radial distribution function $F(R)$ was calculated by the Fourier transformation of $k^3w(k)\chi(k)$ in the 2−14 Å$^{-1}$ range; $w(k)$ is a Kaiser−Bessel apodization window with smoothness coefficient $\tau = 3$. After Fourier filtering, the first single-shell Fe−N$_6$ was fitted in the 4−12 Å$^{-1}$ range to the standard EXAFS formula, in a single scattering scheme:

(44) Cantin, C.; Kliava, J.; Marbeuf, A.; Mikaïlitchenko, D. *Eur. Phys. J. B* **1999**, *12*, 525–540.
(45) Kahn, O.; Martinez, J. *Science* **1998**, *279*, 44–48.
(46) (a) Michalowicz, A. *Logiciels pour la Chimie*;Société Française de Chimie: Paris, 1991, 102;(b) Michalowicz, A. *J. Phys. IV* **1997**, *7*, 235.

$$k_\chi(k) = -S_0^2 \sum_{i-1.5} \left[ \frac{N_i}{R_2^i} |(F\pi, k)| e^{-2\sigma^2 k^2} e^{-\frac{2R}{\lambda(k)}} \sin(2kR_i + 2\partial_1 + \Psi(k)) \right] (4)$$

where $\&S^2_0$ is the inelastic reduction factor, $N$ is the number of nitrogen atoms at the distance $R$ from the iron center, $\lambda(k)$ is the mean free path of the photoelectron, $\sigma$ is the Debye−Waller factor, giving the width of the Fe−N distance distribution, $\partial_1(k)$ is the central atom phase shift, and $|(F\pi,k)|$ and $\Psi(k)$ the amplitude and phase of the nitrogen back-scattered wave. The curve-fitting analysis for the first coordination sphere of the iron was performed with *Round Midnight*[47] code after Fourier filtering in the 0.7−2.0 Å range of the EXAFS spectrum. Spherical-wave theoretical amplitudes and phase shifts calculated by the *McKale*[48] code were used. Because theoretical phase shifts were used, we fitted the energy threshold $E_0$, ($\Delta E_0$). The goodness of fit was given by:

$$\rho(\%) = \frac{\Sigma[k\chi_{\exp}(k) - k\chi_{th}(k)]^2}{\Sigma[k\chi_{\exp}(k)]^2} \quad (5)$$

**Synthesis of Materials.** Starting reagents and solvents were obtained commercially from Aldrich or Acros and used as received.

**General Procedure for the Synthesis of $C_n$-1 and $C_n$-3.** To a hot methanolic solution of 3,5-dialkoxy-*N*-4*H*-1,2,4-triazol-4-ylbenzamide[12a,b] was added a methanolic solution of the $FeX_2 \cdot 6H_2O$ ($X = CF_3SO_3^-$, $BF_4^-$). The mixture was refluxed for 5 min, then concentrated by evaporating and allowed to cool to room temperature. The precipitate of a complex was filtered off and dried in air.

**Triflate Series. $C_4$-1.** $C_4$tba (0.215 g, 0.648 mmol), $Fe(CF_3SO_3)_2 \cdot 6H_2O$ (0.1 g, 0.216 mmol); Anal. Calcd for $C_{53}H_{73}F_6FeN_{12}O_{15.5}S_2$: C, 46.80, H, 5.41, N, 12.36, S, 4.71. Found C, 46.53, H, 5.22, N, 12.03, S, 4.39.

**$C_6$-1.** $C_6$tba (0.251 g, 0.648 mmol), $Fe(CF_3SO_3)_2 \cdot 6H_2O$ (0.1 g, 0.216 mmol); Anal. Calcd for $C_{65}H_{97}F_6FeN_{12}O_{15.5}S_2$: C, 51.08, H, 6.40, N, 11.00, S, 4.20. Found C, 51.02, H, 6.84, N, 10.59, S, 4.30.

**$C_8$-1.** $C_8$tba (0.288 g, 0.648 mmol), $Fe(CF_3SO_3)_2 \cdot 6H_2O$ (0.1 g, 0.216 mmol); Anal. Calcd for $C_{77}H_{121}F_6FeN_{12}O_{15.5}S_2$: C, 54.50, H, 7.19, N, 9.91, S, 3.78. Found C, 54.63, H, 7.18, N, 9.80, S, 3.62.

**$C_{10}$-1.** $C_{10}$tba (0.324 g, 0.648 mmol), $Fe(CF_3SO_3)_2 \cdot 6H_2O$ (0.1 g, 0.216 mmol); Anal. Calcd for $C_{89}H_{145}F_6FeN_{12}O_{15.5}S_2$: C, 57.31, H, 7.84, N, 9.01, S, 3.44. Found C, 57.36, H, 8.19, N, 9.12, S, 3.12.

**$C_{12}$-1.** $C_{12}$tba (0.36 g, 0.648 mmol), $Fe(CF_3SO_3)_2 \cdot 6H_2O$ (0.1 g, 0.216 mmol); Anal. Calcd for $C_{101}H_{169}F_6FeN_{12}O_{15.5}S_2$: C, 59.66, H, 8.38, N, 8.27, S, 3.15. Found C, 59.96, H, 8.54, N, 8.28, S, 3.27.

**Tetraflouroborate series. $C_4$-3.** $C_4$tba (0.295 g, 0.888 mmol), $Fe(BF_4)_2 \cdot 6H_2O$ (0.1 g, 0.296 mmol); Anal. Calcd for $C_{51}H_{74}B_2F_8FeN_{12}O_{10}$: C, 49.21, H, 5.99, N, 13.50. Found C, 49.20, H, 6.29, N, 13.20.

**$C_6$-3.** $C_6$tba (0.344 g, 0.888 mmol), $Fe(BF_4)_2 \cdot 6H_2O$ (0.1 g, 0.296 mmol); Anal. Calcd for $C_{63}H_{98}B_2F_8FeN_{12}O_{10}$: C, 53.55, H, 6.99, N, 11.90. Found C, 53.18, H, 6.81, N, 11.66.

**$C_8$-3.** $C_8$tba (0.395 g, 0.888 mmol), $Fe(BF_4)_2 \cdot 6H_2O$ (0.1 g, 0.296 mmol); Anal. Calcd for $C_{75}H_{122}B_2F_8FeN_{12}O_{10}$: C, 56.97, H, 7.78, N, 10.63. Found C, 56.50, H, 7.42, N, 10.51.

**$C_{10}$-3.** $C_{10}$tba (0.444 g, 0.888 mmol), $Fe(BF_4)_2 \cdot 6H_2O$ (0.1 g, 0.296 mmol); Anal. Calcd for $C_{87}H_{146}B_2F_8FeN_{12}O_{10}$: C, 59.72, H, 8.41, N,9.61. Found C, 59.89, H, 8.37, N, 9.37.

**$C_{12}$-3.** $C_{12}$tba (0.494 g, 0.888 mmol), $Fe(BF_4)_2 \cdot 6H_2O$ (0.1 g, 0.296 mmol); Anal. Calcd for $C_{99}H_{170}B_2F_8FeN_{12}O_{10}$: C, 62.00, H, 8.93, N, 8.76. Found C, 61.87, H, 8.68, N, 8.47.

**Acknowledgment.** We acknowledge the financial help from the Deutsche Forschungsgemeinschaft (Priority Program 1137 "Molecular Magnetism"), the Fonds der Chemischen Industrie. A.B.G. thanks the Spanish MEC for a Ramon y Cajal research contract, for the project CTQ 2007-64727 and the Alexander von Humboldt Foundation for work-visiting fellowships. Y.G. acknowledges the financial support from the DLR/BMBF project RUS 05/003 and RFBR grant 03-03-32571. We also thank Ms. E. Muth and Ms. P. Räder of the Max-Planck-Institute for Polymer Research, Mainz, for their help in performing TGA and DSC measurements, and Dr. Gutmann and Mr. M. Bach for help in performing temperature-dependent XRPD measurements. We also acknowledge the support of the responsible scientist Dr. E. Welter from HASYLab and Dr. H. Ehrenberg and Dominic Stürmer from TU Darmstadt during the EXAFS measurements at beamline A1 and A. Michalowicz for providing us with his XAS analysis package.[47]

**Supporting Information Available:** This material is available free of charge via the Internet at http://pubs.acs.org.

IC8006266

(47) (a) Michalowicz in, A. *Logiciels pour la Chimie*; Société Française de Chimie: Paris, 1991, 116.

(48) (a) McKale, A. G.; Knapp, G. S.; Chan, S.-K. *Phys. Rev. B* **1986**, *33*, 841. (b) McKale, A. G.; Veal, B. W.; Paulikas, A. P.; Chan, S.-K.; Knapp, G. S. *J. Am. Chem. Soc.* **1988**, *110*, 3763.